(article starts on next page)

❙ Research Article

Disorder-Induced Transitions in Topological Phases of the Hofstadter Model

Junais Habeeb Mokkath[1,2] 🔵

[1]College of Integrative Studies, Abdullah Al Salem University (AASU), Khaldiya, Kuwait | [2]Department of Applied Physics, Chalmers University of Technology, Gothenburg, Sweden

Correspondence: Junais Habeeb Mokkath (junais.mokkath@aasu.edu.kw)

ABSTRACT

Topological phases of matter are known for their robustness against perturbations, yet their stability under disorder remains an open question of both theoretical and experimental relevance. We study the disordered Hofstadter model, where magnetic flux generates fractal minibands carrying nontrivial Chern numbers. Using numerical simulations, we construct a disorder–flux phase diagram by computing Chern numbers and gap statistics across a wide range of parameters. We find that weak to moderate disorder preserves quantized Chern phases, while strong disorder closes mobility gaps, induces Chern-number fluctuations, and drives transitions to trivial insulating states. Our results provide direct guidelines for engineering disorder and flux in synthetic lattices, with implications for quantum simulation and quantum device design.

1 | Introduction

Topological phases of matter have reshaped our understanding of electronic systems, revealing robust phenomena insensitive to local perturbations [1–6]. Among the earliest theoretical realizations of such phases is the Hofstadter model, which describes electrons on a two-dimensional lattice subjected to a perpendicular magnetic field [7]. The resulting energy spectrum, known as the Hofstadter butterfly, exhibits a fractal structure composed of magnetic minibands characterized by nontrivial Chern numbers [2]. These topological invariants underlie quantized Hall conductance and are central to the classification of Chern insulators. While much progress has been made in understanding topological phases in clean systems, real materials inevitably host disorder. Disorder can dramatically alter topological behavior–suppressing, preserving, or even inducing topological phases in systems where they were absent [8]. This dual role of disorder is exemplified by the topological Anderson insulator (TAI) [8], where disorder facilitates a transition into a topologically nontrivial state. However, the broader landscape of

disorder effects in lattice models with magnetic flux, such as the Hofstadter model, remains only partially explored.

Recent studies have also highlighted that disorder can play a constructive rather than merely destructive role in shaping topological matter. In particular, disorder-induced higher-order topological insulators have been shown to emerge in systems where clean-limit topology is absent, revealing that randomness itself can give rise to quantized edge or corner modes and robust boundary responses. For example, Liu et al. [9] demonstrated experimentally in circuit-based lattices that disorder can generate higher-order topological states. These findings complement our results on disorder-stabilized Chern phases in the Hofstadter model, illustrating the broader principle that controlled disorder can serve as a tuning knob for realizing and manipulating nontrivial topology in engineered quantum systems.

In this work, we systematically investigate how on-site disorder modifies the spectral and topological properties of the Hofstadter

model. Using the Fukui–Hatsugai–Suzuki method [10] (FSH), we compute the Chern number of the lowest energy band across a wide range of magnetic flux values and disorder strengths. By constructing a topological phase diagram and analyzing energy gap statistics, we reveal the conditions under which topological protection breaks down. In addition, we examine fluctuations of the Chern number across disorder realizations, providing insight into the stability and resilience of Chern phases under increasing randomness. Our results not only deepen theoretical understanding of disorder-driven topological transitions but also provide experimentally relevant benchmarks for platforms such as ultracold atomic lattices, moiré heterostructures, and photonic crystals, where tunable disorder and synthetic gauge fields can be engineered with high precision. The interplay between disorder, topology, and localization explored here sheds light on the fundamental limits of topological protection in quantum matter.

2 | Computational Methodology

In this work, our research object is the disordered Hofstadter model, a paradigmatic lattice Hamiltonian for studying Chern phases in the presence of magnetic flux and on-site disorder, rather than a specific material realization. For rational flux $\phi = p/q$, we adopt a magnetic unit cell of size q so that magnetic translation symmetry is restored and a well-defined magnetic Brillouin zone exists. All momentum-space calculations (e.g., band structures and Chern numbers) are performed with q matched to the denominator of ϕ for each data point. In momentum-space treatments of the Hofstadter model, a magnetic Brillouin zone exists only when the magnetic unit cell size equals the denominator q of $\phi = p/q$. Accordingly, all momentum-space results shown here use a unit cell matched to q for each ϕ. When disorder is present and band labels are not globally well-defined, we rely on real-space/topological subspace diagnostics to establish phase boundaries.

The magnetic field is incorporated using the Landau gauge via Peierls phase factors [11] in the hopping terms. The clean Hamiltonian is written as:

$$H = -t \sum_{m,n} \left(c_{m+1,n}^{\dagger} c_{m,n} + e^{i2\pi\phi m} c_{m,n+1}^{\dagger} c_{m,n} + \text{h.c.} \right), \quad (1)$$

where t is the nearest-neighbor hopping amplitude, and $c_{m,n}^{\dagger}$ creates an electron at site (m, n). The introduction of magnetic flux leads to a magnetic unit cell of size q, and the system exhibits q energy bands.

To simulate disorder, we add a uniform random on-site potential drawn from the interval $[-W/2, W/2]$, where W/t represents the disorder strength. The resulting disordered Hamiltonian is then diagonalized numerically for various combinations of flux ϕ and disorder W. We compute the Chern number of the lowest energy band using the FHS method, a gauge-invariant and numerically stable discretization of Berry curvature over a finite Brillouin zone grid. The momentum-space Hamiltonian $H(\mathbf{k})$ is computed at each grid point (k_x, k_y), and the eigenvectors of the band of interest are extracted.

TABLE 1 | Parameters used for the Hofstadter model simulations. The flux is given by $\phi = p/q$, where p is the numerator and q the denominator of the rational flux fraction.

Parameter	Value/Description
Flux per plaquette (ϕ)	20 values in (0.01, 0.49]
Disorder strength (W/t)	20 values in [0.0, 4.0]
Disorder distribution	Uniform in $[-W/2, W/2]$
Disorder averaging	10–20 independent realizations per point
BZ discretization ($n_k \times n_k$)	32×32 grid points
Bands analyzed	Lowest band ($n = 0$)
Gap definition	$\Delta E = E_1 - E_0$ at each $\mathbf{k}$
Chern method	Fukui-Hatsugai-Suzuki (FHS) method
Diagonalization method	Dense matrix diagonalization (numpy.linalg.eigh)

The discretized Berry curvature is computed on each plaquette via the link variables:

$$F_{xy}(\mathbf{k}) = \text{Im}\left[\log U_x(\mathbf{k}) U_y(\mathbf{k} + \hat{x}) U_x^{-1}(\mathbf{k} + \hat{y}) U_y^{-1}(\mathbf{k}) \right], \quad (2)$$

where $U_\mu(\mathbf{k}) = \langle u(\mathbf{k}) | u(\mathbf{k} + \hat{\mu}) \rangle$ are the overlaps of neighboring Bloch eigenvectors. The total Chern number is obtained as:

$$C = \frac{1}{2\pi} \sum_{\mathbf{k}} F_{xy}(\mathbf{k}). \quad (3)$$

For each (ϕ, W) pair, we perform multiple disorder realizations and compute both the mean and standard deviation of the Chern number to assess the topological robustness.

2.1 | Conventions and Units

Throughout this work, all energies are expressed in units of the nearest-neighbor hopping t. Accordingly, we report and plot the *disorder strength* as the dimensionless ratio W/t. We reserve the plain symbol W only when stating an explicit equality (e.g., $W = 1.5\,t$) or when defining the bare on-site distribution $\epsilon_i \in [-W/2, W/2]$. Figures, axes, and captions therefore use W/t (and, where relevant, E/t and ϕ/ϕ_0) for consistency.

To probe the stability of the topological phase, we compute the energy gap between the lowest and first excited bands as a function of disorder. This is achieved by direct diagonalization of the Hamiltonian at each momentum point and extracting $\Delta E = E_1 - E_0$. The regions where ΔE vanishes serve as indicators of topological phase transitions. We overlay these gap-closing contours onto the Chern number phase diagram. The Brillouin zone is discretized into a 32×32 grid for the Fukui method. We scan disorder strengths $W \in [0, 4]$ and flux values $\phi \in (0, 0.5)$, using a grid of 20×20 points, see Table 1. Each data point is averaged over 10–20 disorder realizations. To confirm that this sampling is sufficient for statistically meaningful results, we performed convergence tests by increasing the number of

realizations up to $N_{dis} = 20$ for representative parameter sets. The mean and standard deviation of key observables—such as the Chern number $\langle C \rangle$ and the average band gap $\langle \Delta E \rangle$—changed by less than 5% when increasing the number of realizations beyond ten. This confirms that averaging over 10–20 disorder configurations yields statistically stable and reproducible results within numerical accuracy. We diagonalize the Hamiltonians using standard linear algebra routines for small dense matrices. All energies, including the disorder strength W/t, are expressed in units of the nearest-neighbor hopping amplitude t. The magnetic flux per plaquette is written as $\phi = p/q$ in units of the flux quantum $\phi_0 = h/e$, and is therefore dimensionless. Accordingly, in all figures we label the axes as W/t, ϕ/ϕ_0, and E/t where appropriate.

2.2 | Why the Hofstadter Model for Disorder–Topology?

The Hofstadter model offers a controlled and symmetry-lean framework in which magnetic flux produces fractal minibands endowed with quantized Chern numbers. Working at rational flux $\phi = p/q$ restores a magnetic Brillouin zone and permits robust FHS evaluation of Chern numbers on a finite grid while scanning disorder strength. This enables a global (ϕ, W) stability map that integrates (i) gap statistics, revealing a non-monotonic disorder response, with (ii) fluctuation diagnostics of the Chern number that flag mobility-gap closure and the onset of ill-defined momentum-space invariants. Crucially, the same ingredients are realizable in ultracold-atom, moiré, and photonic platforms–where synthetic gauge fields and controlled disorder are routine–allowing direct parameter translation and experimental validation of our predictions.

2.2.1 | Validity of the FHS Method Under Strong Disorder

The FHS algorithm relies on a well-defined mobility gap that separates occupied and unoccupied states on a discretized Brillouin zone [10]. At weak and moderate disorder ($W/t \lesssim 3$), this condition is satisfied and the computed Chern numbers are quantized within numerical precision. However, when $W/t \gtrsim 3$, the disorder potential closes the mobility gap and induces significant band intermixing. In this regime, Anderson localization dominates, extended Bloch states cease to exist, and the FHS formula no longer represents a true topological invariant. Accordingly, the fluctuating "average Chern numbers" reported for large W/t should be interpreted as numerical indicators of phase instability rather than as physically meaningful Chern integers.

3 | Results and Discussion

We model on-site disorder by adding a random potential ϵ_i at each lattice site, drawn from a uniform distribution $\epsilon_i \in [-W/2, W/2]$, where W denotes the disorder strength. Throughout this work, energies are expressed in units of the nearest-neighbor hopping amplitude t, so that W is dimensionless. In Figure 1, we fix $W = 1.5\,t$ as a representative intermediate disorder strength: this choice is large enough to substantially modify the Hofstadter
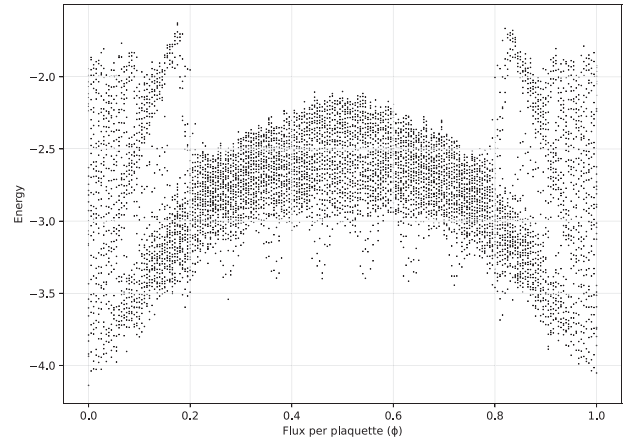

FIGURE 1 | Hofstadter spectrum at disorder strength $W/t = 1.5$, showing band broadening and partial gap closure due to disorder while retaining remnants of the fractal structure. Energies are in E/t and flux in ϕ/ϕ_0.

spectrum and induce band mixing, but not so strong as to fully localize all states. While there is no unique "optimal" value of W, selecting a moderate value highlights the competition between topological band structure and disorder in a regime of experimental relevance. First, we present the Hofstadter spectrum under the influence of disorder with a disorder strength of $W = 1.5$, see Figure 1. The plot shows the energy eigenvalues as a function of the magnetic flux per plaquette ϕ, capturing the intricate behavior of the energy bands. It is well known that, in the absence of disorder, the Hofstadter butterfly displays a fractal and highly symmetric structure [7]. However, the inclusion of disorder leads to a broadening and smearing of the spectral features [12,13]. Notably, vestiges of the original butterfly structure remain visible, particularly near the center of the energy spectrum, suggesting a partial retention of the system's topological characteristics [14]. The data also reveal the presence of localized states and evolving energy gaps as a function of ϕ, underscoring the rich interplay between magnetic field effects and disorder in quantum lattice systems.

3.1 | Quantitative Disorder Regimes

To make our terminology precise within the present numerical setup (32×32 Brillouin-zone grid; 10–20 disorder realizations per point; see Table 1), we classify disorder into three operational regimes:

- **Weak**: $W/t < 1.5$. The mobility gap remains open across the k-grid; $\langle \Delta E \rangle$ is near the clean value and often slightly enhanced; the Chern number is quantized with negligible fluctuations ($std[C] \lesssim 0.5$).

- **Moderate**: $1.5 \leq W/t \leq 3.0$. The average gap decreases and begins to show non-monotonic behavior (peak near $W/t \approx 3.2$), reflecting competition between level repulsion and localization; Chern-number fluctuations increase but a mobility gap still persists ($std[C] \lesssim 2$).
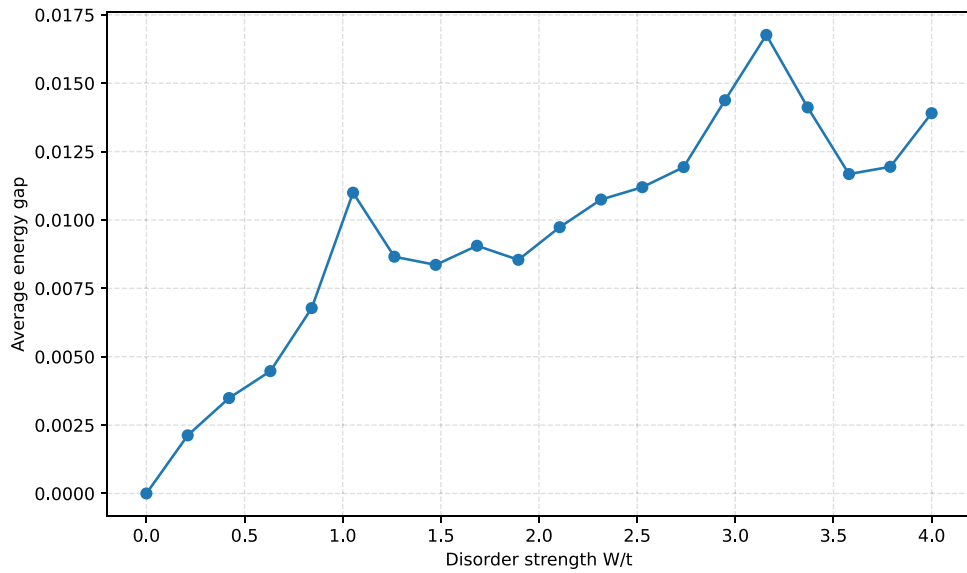
FIGURE 2 | Average band gap $\langle \Delta E \rangle$ of the Hofstadter model versus disorder strength W/t (scan range [0,4]). The gap shows a non-monotonic response with a maximum near $W/t \approx 3.2$, reflecting competition between disorder-enhanced level repulsion and localization; for $W/t \gtrsim 3$, mobility-gap closure begins to suppress $\langle \Delta E \rangle$.

- **Strong**: $W/t > 3.0$. Gap-closure events and Anderson localization render momentum-space band identities ill-defined; in this regime, FHS-based "Chern numbers" are no longer topological invariants and should be interpreted only as numerical indicators of phase instability.

Building upon the qualitative spectral broadening seen in Fig. 1, we now quantitatively analyze how disorder affects the energy separation between bands, see Figure 2. This allows us to assess the stability of the spectral gaps and their role in supporting topological phases. The results reveal a non-monotonic dependence of the average energy gap on W: the gap initially increases with disorder, reaching a local maximum near $W \approx 3.2$, before slowly diminishing at higher disorder strengths. The non-monotonic behavior of the average energy gap as a function of disorder strength (W/t) reflects the interplay between two competing mechanisms: level repulsion and localization [15]. At weak to moderate disorder, disorder-induced mixing of closely spaced energy levels can enhance spectral repulsion, leading to the opening or widening of small gaps that may be closed in the clean limit. This effect, often overlooked, results from the redistribution of spectral weight and can temporarily stabilize energy gaps by suppressing degeneracies [8,14]. However, as disorder increases further, this trend reverses. The growing randomness in the on-site potential leads to significant band broadening, increasing overlap between adjacent bands and promoting the proliferation of in-gap states [16]. These in-gap states destabilize the quantized band topology and drive the system toward gap closure. Eventually, strong disorder induces Anderson localization, where electronic wavefunctions become spatially confined and the system loses its coherent band structure altogether [13,15]. In this regime, the concept of a well-defined energy gap–and thus a well-defined Chern number–becomes increasingly ill-posed. Therefore, the observed peak in the average gap at intermediate W marks a crossover between disorder-enhanced gap opening and disorder-driven topological collapse. For W/t beyond the range shown, disorder continues to broaden the spectrum and
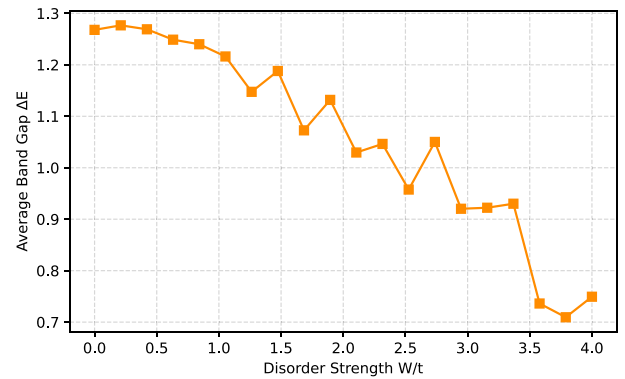

FIGURE 3 | Average band gap ΔE vs disorder strength W/t at fixed flux $\phi = 0.33$; ΔE is reported in E/t. The band gap remains stable for weak disorder and decreases significantly beyond $W \approx 2.5$, signaling gap closing and possible localization effects.

seed in-gap states, leading to progressive mobility-gap closure. Consequently, the k-resolved band separation $\Delta E = E_1 - E_0$ does not saturate at its clean value; instead it trends downward toward zero (up to finite-size/grid limits). In this regime Anderson localization dominates and momentum-space band identities become ill-defined, so ΔE and FHS-based Chern numbers lose their topological meaning [10].

Figure 3 illustrates the behavior of the average band gap ΔE as a function of disorder strength W/t for a fixed magnetic flux $\phi = 0.33$. The data show that the band gap remains relatively stable up to moderate disorder levels $W \lesssim 1.5$, with only minor fluctuations in ΔE. Beyond this regime, a gradual decline in the band gap is observed, indicating the increasing influence of disorder on electronic coherence and band separation. Notably, for $W \gtrsim 2.5$, the band gap begins to collapse more rapidly, accompanied by pronounced fluctuations. This sharp suppression of ΔE is consistent with the onset of Anderson localization and gap
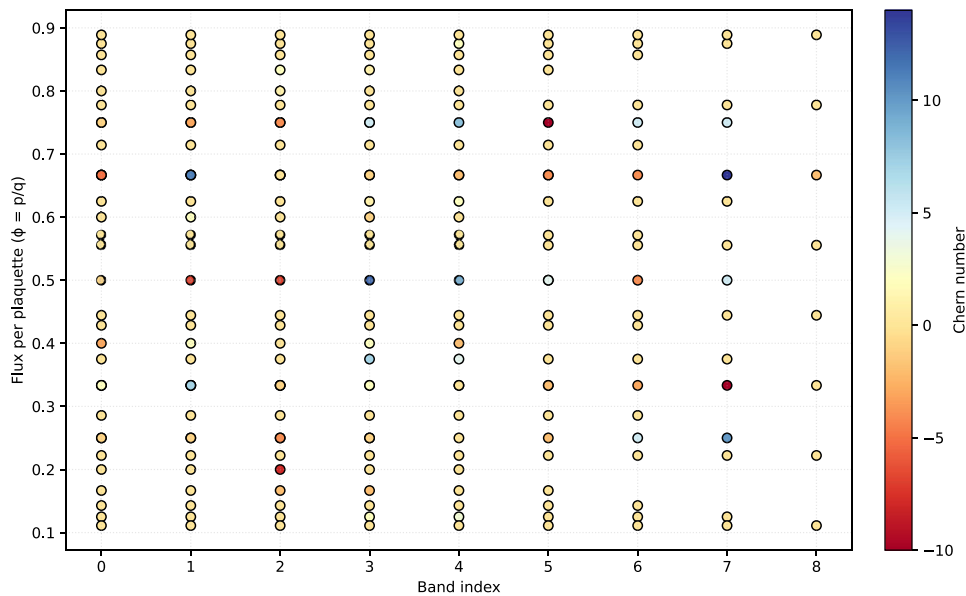
FIGURE 4 | Chern numbers assigned to each energy band as a function of magnetic flux per plaquette $\phi = p/q$. Color indicates the integer value of the Chern number, with positive (blue) and negative (red) values marking distinct topological phases.

closing phenomena that disrupt the topological band structure [17,18]. These results highlight the fragility of spectral gaps to disorder and suggest a disorder-driven transition from a gapped topological phase to a localized regime [19].

While energy gaps offer a direct window into possible topological transitions, the Chern number provides a topological invariant that directly characterizes phase robustness. To gain insight into the baseline topological structure, we begin by examining the distribution of Chern numbers in the clean limit. Figure 4 presents the distribution of Chern numbers across all energy bands as a function of magnetic flux per plaquette, $\phi = p/q$, in a lattice system exhibiting quantum Hall physics. Each colored marker denotes the Chern number assigned to a specific energy band at a given rational flux value. The results clearly demonstrate the topological complexity of the Hofstadter model, where band structures reorganize in response to changes in magnetic flux, giving rise to a rich sequence of quantized Chern numbers [20–22]. The alternation and clustering of positive and negative values reflect the intricate interplay between magnetic translation symmetry and band topology. The persistence of nonzero Chern numbers over a broad range of fluxes indicates the robustness of topological order in the presence of lattice periodicity. The associated color scale highlights the magnitude and sign of the Chern numbers, revealing how band topology evolves discontinuously across gaps in the energy spectrum. These features serve as a hallmark of topologically nontrivial phases and are essential for understanding quantized transport phenomena in systems subjected to magnetic fields.

Next, we turn to the full topological phase diagram as a function of flux and disorder strength. Figure 5 displays the evolution of Chern numbers in the lowest energy band of the Hofstadter model as a function of both magnetic flux per plaquette ϕ and disorder strength W/t. The color map encodes the computed Chern number, with red and blue regions indicating negative and positive topological invariants, respectively. At low disorder

($W \approx 0$), the system exhibits sharply defined regions of quantized Chern numbers consistent with the clean Hofstadter butterfly. As W increases, disorder induces fluctuations and irregularities in the topological indices, reflecting the breakdown of global topological protection and the emergence of localized states [23]. Remarkably, even at moderate disorder strengths, well-defined Chern plateaus persist in certain flux intervals, demonstrating the robustness of topological order to perturbations [24]. However, beyond $W \approx 3$, the proliferation of topological transitions and the suppression of quantized values signal the approach to a topologically trivial regime, where gap closings and spectral mixing become prevalent. This figure highlights the rich and complex interplay between magnetic field, disorder, and topology in two-dimensional lattice systems.

While the phase diagram reveals the average Chern number across parameter space, it does not capture the degree of variation induced by disorder. To assess the stability of these topological regions, we compute the standard deviation of the Chern number across disorder realizations. Figure 6 shows the standard deviation of the Chern number as a function of disorder strength W/t and magnetic flux per plaquette ϕ. The fluctuations in the Chern number across disorder realizations, as quantified by the standard deviation, serve as a diagnostic of topological phase stability. In clean systems or those with weak disorder, the Chern number is quantized and invariant under small perturbations, reflecting robust topological protection. However, as disorder strength increases, especially near critical points where energy gaps close, local variations in the electronic structure lead to sample-dependent reconfigurations of the Berry curvature. This results in fluctuations in the computed Chern number, signaling the breakdown of global topological order. Physically, this can be interpreted as the coexistence of localized and delocalized states near the mobility edge, where the topological invariant becomes ill-defined due to the lack of a uniform gap across the Brillouin zone. Thus, the standard deviation not only tracks numerical instability but also captures the intrinsic fragility of topological indices in disordered systems [25].
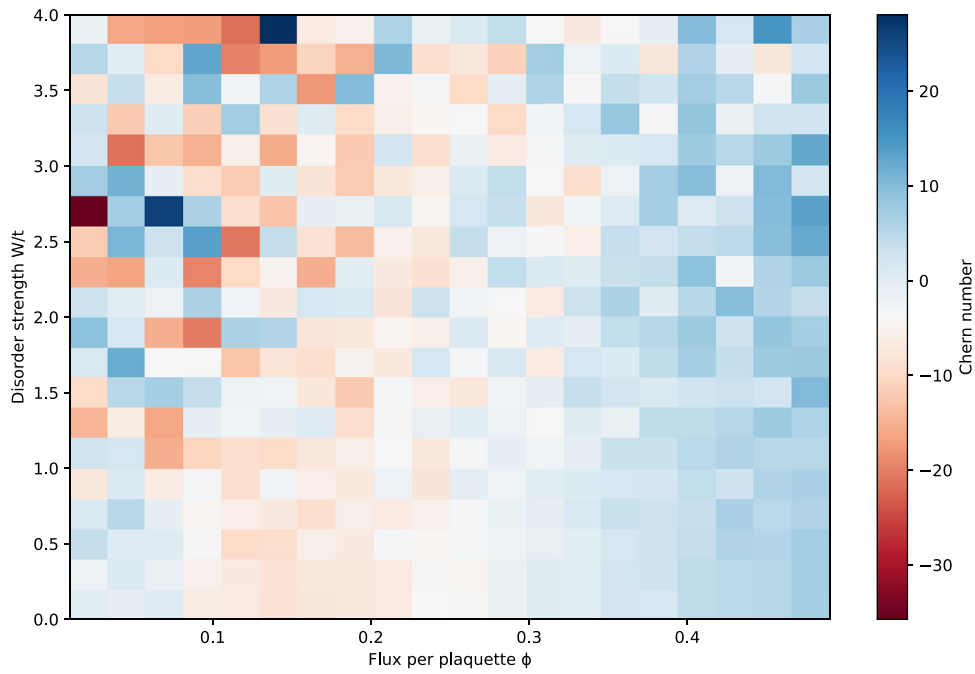
FIGURE 5 | Chern number as a function of flux per plaquette ϕ and disorder strength W/t. Colors represent the topological invariant associated with each parameter set, with red and blue corresponding to negative and positive Chern numbers, respectively.
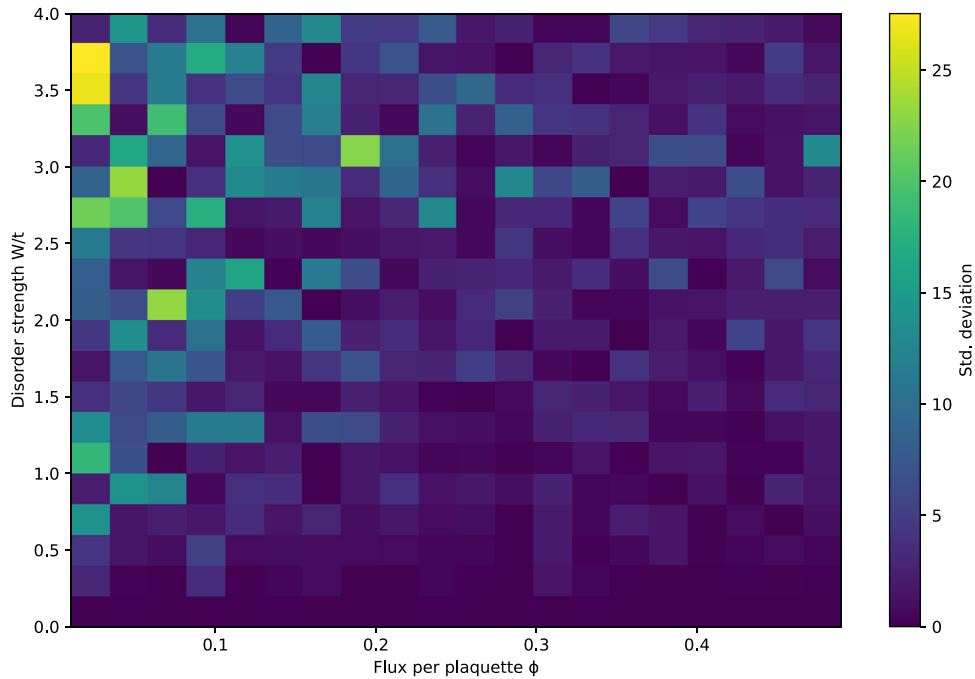

FIGURE 6 | Standard deviation of the Chern number as a function of disorder strength W/t and magnetic flux per plaquette ϕ. The color map indicates the variability of the topological index across disorder realizations, highlighting regions of increased topological instability.

The disorder-induced transitions observed in the disordered Hofstadter model bear notable similarities to those in the Topological Anderson Insulator (TAI), originally identified in time-reversal symmetric systems with spin-orbit coupling [8,26]. In both cases, disorder plays a nontrivial dual role–stabilizing topological phases in certain regimes while suppressing them in others.

In the Hofstadter model, we observe regions where moderate disorder preserves or even enhances quantized Chern numbers, analogous to the disorder-enabled topological states in TAI systems. However, a key distinction lies in the underlying symmetry: the Hofstadter model breaks time-reversal symmetry and lacks spin degrees of freedom, precluding a direct realization of TAI
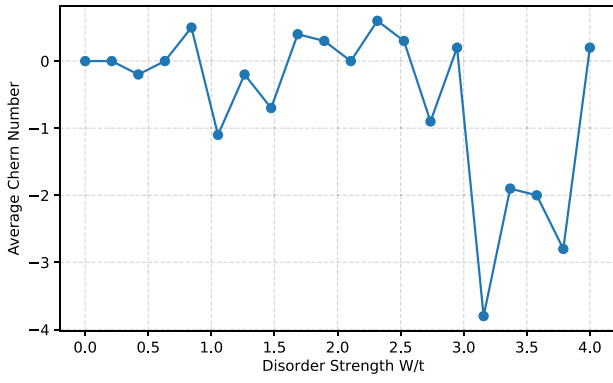
FIGURE 7 | Average Chern number of the lowest energy band as a function of disorder strength W/t at fixed magnetic flux $\phi = 0.33$. The results are averaged over multiple disorder realizations.

FIGURE 8 | Standard deviation of the Chern number as a function of disorder strength W/t for fixed magnetic flux $\phi = 0.33$. Increased variability at larger W reflects reduced topological stability due to disorder.

as defined in Z_2-invariant systems. Nevertheless, the qualitative features–non-monotonic gap behavior, disorder-stabilized topological plateaus, and eventual topological breakdown–underscore a universal mechanism by which disorder reshapes the topological phase landscape, independent of specific symmetry classes.

Figure 7 reveals the spread of topological outcomes at fixed disorder, but averaging over realizations provides a broader view of the disorder-induced evolution. We next examine the mean and variance of the Chern number as functions of W at fixed flux. In this context, Figure 7 depicts the average Chern number of the lowest energy band as a function of disorder strength W/t for a fixed magnetic flux per plaquette $\phi = 0.33$. Each data point represents an average over multiple disorder realizations to capture the statistical response of the topological invariant under increasing randomness. For small disorder strengths ($W \lesssim 1.0$), the Chern number remains close to zero with modest fluctuations, indicating a topologically trivial or weakly perturbed phase. As W increases beyond this regime, the Chern number exhibits strong fluctuations and intermittent drops to negative values, suggesting the emergence of disorder-induced topological transitions and breakdown of quantized behavior [27–29]. Particularly beyond $W \approx 3.0$, the average value becomes increasingly negative and erratic, reflecting significant spectral mixing and localization effects. This transition illustrates the fragile nature of topological order in the Hofstadter model and underscores the importance of disorder in driving topological phase instability.

Figure 8 shows the standard deviation of the Chern number as a function of disorder strength W/t for a fixed magnetic flux $\phi = 0.33$. This measure quantifies the variability of the topological index across multiple disorder realizations, serving as a proxy for the stability and robustness of topological phases. At low disorder, the standard deviation remains near zero, consistent with well-quantized Chern numbers and minimal sample-to-sample fluctuations. As W increases, the standard deviation gradually rises, with a sharp increase observed beyond $W \approx 2.5$, indicating enhanced topological instability and phase randomness. This behavior reflects the increasing influence of disorder on the electronic structure, particularly the collapse of well-defined energy gaps and the proliferation of topological transitions. The
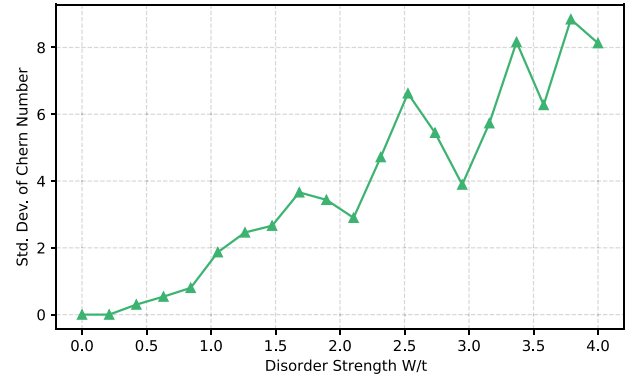
trend supports the conclusion that moderate to strong disorder not only modifies the average Chern number but also undermines its reliability as a robust quantized invariant [30].

3.2 | Interpreting $\langle C \rangle$ at Strong Disorder

The FHS Chern number is well defined only when a mobility gap separates occupied from unoccupied states. Consequently, for $W/t \gtrsim 3$—where gap closing, band intermixing, and Anderson localization set in—the momentum-space Chern number loses topological meaning. In this regime the quantity plotted in Figure 7 should therefore be read as a numerical indicator of phase instability rather than a quantized invariant, consistent with the surge of fluctuations in Figure 8. This interpretation aligns with our discussion of disorder-driven gap collapse and the ill-posed nature of band Chern numbers at strong disorder.

To assess the experimental accessibility of our results, we translate the dimensionless parameters of the Hofstadter model into realistic energy scales for state-of-the-art quantum simulation platforms. In our simulations, all quantities are expressed in units of the nearest-neighbor hopping amplitude t. Typical values of t vary widely across physical realizations, from kilohertz scales in ultracold atomic lattices to millielectronvolts in moiré graphene systems. This mapping enables a direct comparison between our disorder–flux phase diagram and experimentally tunable regimes. In optical lattice experiments, the tunneling amplitude is typically on the order of a few kilohertz ($1t \approx 3\,\text{kHz} \approx 150\,\text{nK}$) [31,32]. Accordingly, the disorder strength range studied here ($W \in [0, 4]t$) corresponds to an energy window of 0–600 nK, well within the reach of current techniques that generate controlled disorder using laser speckle fields or programmable digital micromirror devices [33,34]. The smallest gaps observed in our calculations ($\Delta E \sim 0.01t$) correspond to a few nanoKelvin, which is within the resolution of cold-atom spectroscopy methods such as band mapping or quench dynamics [35]. These estimates indicate that both the disorder-induced enhancement of spectral gaps and their eventual collapse at strong disorder are observable with current cold-atom technology. In moiré superlattices such as twisted bilayer graphene, the tunneling energy is much

larger, typically $t \sim 10$ meV. In this case, the same disorder window maps to 0–40 meV. The characteristic gap sizes of $\Delta E \sim 0.015t$ correspond to ~ 0.15 meV, which is directly resolvable by scanning tunneling microscopy (STM) and quantum Hall transport [36–38]. Notably, the predicted disorder-driven transitions occur at comparable energy scales to those already probed in graphene moiré experiments, making this a promising solid-state setting for testing our predictions. Finally, in photonic lattices, Hofstadter physics can be simulated using dielectric resonator arrays or waveguide lattices with engineered couplings. Here, disorder can be introduced by controlled variations in refractive index or waveguide widths. The effective hopping amplitudes in such systems are typically in the GHz frequency range, implying that our predicted disorder thresholds correspond to easily implementable fabrication tolerances. Moreover, photonic lattices provide an opportunity to probe disorder-induced transitions through direct imaging of localized versus delocalized optical modes [39].

3.3 | Relation to Prior Work

The robustness of Chern phases against weak disorder is a foundational result in the quantum Hall and Chern–insulator literature, established by seminal and subsequent studies.[40–42] Our goal here is not to restate this baseline, but to place it within a comprehensive stability landscape for the Hofstadter model. In particular, the present work (i) constructs a "global" disorder–flux phase diagram that identifies the regimes of preserved and destroyed topology, (ii) augments it with a quantitative analysis of "gap statistics" that reveals a "non-monotonic" gap response and an intermediate-disorder maximum (Figure 2), together with a physical interpretation in terms of level repulsion competing with disorder-induced localization, (iii) introduces "Chern-number fluctuations" (mean and standard deviation) as a stability diagnostic across flux and disorder (Figures 5–8), clarifying the regime where mobility-gap closure renders momentum-space invariants ill-defined, and (iv) provides a *quantitative mapping* of the dimensionless parameters to experimentally accessible energy scales (ultracold atoms, moiré systems, and photonics), thus delineating concrete windows for observing the predicted crossovers. These additions move beyond the weak-disorder paradigm by delivering a unified, experiment-ready picture that connects disorder-enhanced gaps, fluctuation diagnostics, and topological breakdown within a single disorder–flux stability map.

3.4 | Experimental Implementation Roadmap

Our predictions can be directly tested across several experimental platforms.

3.4.1 | Ultracold Atoms

Hofstadter fluxes can be realized using laser-assisted tunneling or lattice shaking, while on-site disorder is introduced via programmable digital micromirror devices or laser speckle fields. The disorder amplitude W/t can be tuned from 0 to ~ 4 by adjusting the speckle intensity or DMD contrast. Band gaps and Chern numbers may be measured through quench spectroscopy, Hall drift measurements, or Berry-curvature tomography, reproducing the disorder–flux phase diagram in Figures 2–8.

3.4.2 | Moiré Heterostructures

In graphene/hBN superlattices under magnetic fields, rational flux conditions $\phi = p/q$ naturally yield Hofstadter minibands. Controlled potential disorder can be introduced by substrate engineering or local gating, with W/t calibrated from scanning-tunneling spectroscopy. Transport measurements then resolve Chern plateaus and gap suppression with increasing disorder.

3.4.3 | Photonic Lattices

Waveguide or resonator arrays with engineered complex hoppings simulate Hofstadter bands, while controlled refractive-index variations introduce disorder. Edge transport and mode localization directly visualize the topological breakdown predicted at strong disorder.

These platforms together provide a complete and experimentally accessible route to observe the non-monotonic gap evolution, disorder-stabilized Chern phases, and fluctuation-driven topological collapse predicted in this work.

Taken together, the disorder strengths and gap scales identified in our phase diagram are not only theoretically relevant but also experimentally accessible across multiple quantum simulation platforms. Importantly, our results provide specific quantitative benchmarks for the range of disorder values where topological protection is preserved, enhanced, or ultimately destroyed. This positions our work as a practical guide for experimentalists seeking to engineer and probe disorder-driven topological transitions in synthetic quantum systems.

4 | Conclusion and Outlook

In this work we have investigated the stability of Chern phases in the Hofstadter model subject to on-site disorder. Our results suggest that controlled disorder can be used as a knob to stabilize topological phases in regimes that would otherwise be trivial. By computing Chern numbers and energy gap statistics across a wide range of magnetic flux and disorder strengths, we constructed a disorder–flux phase diagram that benchmarks the resilience and eventual breakdown of topological order. Our results show that weak to moderate disorder preserves quantized Chern phases and can even enhance spectral gaps, whereas strong disorder collapses mobility gaps, drives Chern-number fluctuations, and ultimately leads to topologically trivial insulating states. These findings clarify the competing roles of topology and randomness in magnetic lattice systems and provide guidance for synthetic quantum platforms where both flux and disorder can be engineered with high precision, including ultracold atoms, photonic lattices, and moiré heterostructures. Looking ahead, extending this analysis to real-space invariants, mobility-gap diagnostics, and interacting systems would offer a more complete characterization of disorder-driven topological transitions. Such

directions are essential for bridging numerical benchmarks with experimentally accessible observables and for identifying regimes where disorder may be harnessed as a resource to stabilize or induce topological phases.

4.1 | Disorder Engineering and Control

Across experimental platforms, on-site disorder can be parametrized and tuned via the amplitude W/t, spatial correlation length ξ, statistical distribution, and temporal character. Such disorder control has been extensively demonstrated in several synthetic quantum systems. In ultracold atomic lattices, digital micromirror devices or laser speckle fields allow precise amplitude and correlation control of disorder potentials [22,33,35]. In moiré heterostructures, controlled potential disorder is engineered via local gating and substrate engineering, enabling quantitative calibration of W/t through scanning tunneling spectroscopy [36,37]. Photonic lattices implement analogous disorder tuning through designed refractive-index variations and waveguide detunings, providing a direct visualization of disorder-induced localization [39]. Finally, in superconducting circuit arrays, programmable flux biases introduce tunable on-site disorder, making them a reconfigurable platform for exploring disorder–topology interplay [5]. These representative studies establish the experimental feasibility of the disorder-control procedures summarized below and directly motivate the cross-platform comparison presented in this work.

4.1.1 | Ultracold Atoms

Implementation: Add on-site shifts using a digital micromirror device (DMD) or a laser speckle field; ξ set by the DMD pixel size or speckle optics. *Tuning*: Adjust DMD grayscale (or speckle intensity) to sweep $W/t \in [0,4]$; optionally low-pass filter DMD masks to control ξ. *Calibration*: Extract t from Bloch oscillations/band mapping; obtain W from in-situ potential reconstruction or spectroscopy of localized states.

4.1.2 | Moiré Heterostructures

Implementation: Pattern local gates (random masks), engineer controlled strain domains, or introduce calibrated adsorbate/ion-implantation disorder for on-site shifts. *Tuning*: Gate amplitude (rms) sets W; mask features set ξ. *Calibration*: Determine W from STS/SET maps of local potential variance; estimate t from band-structure modeling or quantum oscillations.

4.1.3 | Photonic Lattices

Implementation: Laser-written waveguides or resonator arrays with designed site-frequency detunings; programmable heaters/EOM arrays for reconfigurable disorder. *Tuning*: Fabrication or heater power sets W; lithographic/thermal blur controls ξ. *Calibration*: Retrieve on-site detunings and couplings from spectral/ARPES-like measurements; report W/t from fitted tight-binding parameters.

4.1.4 | Superconducting Circuits

Implementation: Site frequency disorder via flux biases on transmons; tunable couplers set t; optional real-time reprogramming enables ensemble generation. *Tuning*: Flux-noise amplitude (rms) and spatial masks control W, ξ. *Calibration*: Spectroscopy of normal modes yields on-site detunings and t, enabling direct W/t reporting.

4.1.5 | Recommended Procedure

For each platform and target $(\phi, W/t)$: 1) set t; 2) tune disorder amplitude/statistics to hit the desired W/t; 3) fix ξ relative to the lattice spacing a; 4) generate N_{dis} disorder realizations; 5) measure gaps $\Delta E(W/t)$ (spectroscopy) and Chern indicators (Hall drift, plateau sequences, or edge-transport proxies); 6) report mean and standard deviation over the ensemble, enabling one-to-one comparison with our Figures 2–8.

Conflict of Interest

The authors declare no conflict of interest.

Data Availability Statement

The data that support the findings of this study are available from the corresponding author upon reasonable request.

1. Nature Editors, "15 Years of Topological Matter," https://www.nature.com/collections/hhhdhdcgec, 2022, Nature Collection. [Online]. Available: https://www.nature.com/collections/hhhdhdcgec

2. D. J. Thouless, M. Kohmoto, M. P. Nightingale, and M. den Nijs, "Quantized Hall Conductance in A Two-Dimensional Periodic Potential," *Physical Review Letters* 49 (1982): 405–408.

3. Y. Liu, S. Leung, F. Li, Z. Lin, X. Tao, Y. Poo, and J. Jiang, "Bulk–Disclination Correspondence in Topological Crystalline Insulators," *Nature* 589, no. 7842 (2021): 381–385.

4. J. Dobrzyniecki and T. Sowiński, "Simulating Artificial 1d Physics With Ultra-Cold Fermionic Atoms: Three Exemplary Themes," *Advanced Quantum Technologies* 3, no. 6 (2020): 2000010.

5. Z.-Y. Xue and Y. Hu, "Topological Photonics On Superconducting Quantum Circuits With Parametric Couplings," *Advanced Quantum Technologies* 4, no. 9 (2021): 2100017.

6. T. Chen, W. Zhang, D. Zou, Y. Sun, and X. Zhang, "Engineering Topological States and Quantum-inspired Information Processing Using Classical Circuits," *Advanced Quantum Technologies* 8, no. 6 (2025): 2400448.

7. D. R. Hofstadter, "Energy Levels and Wave Functions of Bloch Electrons in Rational and Irrational Magnetic Fields," *Physical Review B: Condensed Matter* 14 (1976): 2239–2249.

8. J. Li, R.-L. Chu, J. K. Jain, and S.-Q. Shen, "Topological Anderson Insulator," *Physical Review Letters* 102 (2009): 136806.

9. S. Liu, H.-X. Zhang, H. Xue, et al., "Disorder-Induced Higher-Order Topological States," *Physical Review Letters* 126 (2021): 146802.

10. T. Fukui, Y. Hatsugai, and H. Suzuki, "Chern Numbers in Discretized Brillouin Zone: Efficient Method of Computing (spin) Hall Conductances," *Journal of the Physical Society of Japan* 74 (2005): 1674–1677.

11. R. Peierls, "Zur Theorie Des Diamagnetismus Von Leitungselektronen," *Zeitschrift für Physik* 80, no. 11 (Nov 1933): 763–791.

12. C. Zhou, M. Berciu, and R. N. Bhatt, "Effects of Large Disorder On The Hofstadter Butterfly," *Physical Review B: Condensed Matter* 71 (Mar 2005): 125310.

13. E. Prodan, "Disordered topological insulators: a non-commutative geometry perspective," *Journal of Physics A: Mathematical and Theoretical* 44, no. 11 (feb 2011): 113001.

14. D. N. Sheng, Z. Y. Weng, L. Sheng, and F. D. M. Haldane, "Quantum spin-hall effect and topologically invariant chern numbers," *Physical Review Letters* 97 (2006): 036808.

15. F. Evers and A. D. Mirlin, "Anderson transitions," *Reviews of Modern Physics* 80, no. 4 (2008): 1355–1417.

16. I. Mondragon-Shem, T. L. Hughes, J. Song, and E. Prodan, "Topological Criticality in the Chiral-Symmetric Aiii Class at Strong Disorder," *Physical Review Letters* 113, no. 4 (2014): 046802.

17. C. W. Groth, M. Wimmer, A. R. Akhmerov, J. Tworzydło, and C. W. Beenakker, "Theory of the Topological Anderson Insulator," *Physical Review Letters* 103, no. 19 (2009): 196805.

18. D. A. Khudaiberdiev, Z. D. Kvon, M. S. Ryzhkov, D. A. Kozlov, N. N. Mikhailov, and A. Pimenov, "Two-Dimensional Topological Anderson Insulator in A Hgte-Based Semimetal," *Physical Review Research* 7 (May 2025): L022033.

19. B.-B. Wang, Z. Cheng, H.-Y. Zou, et al., "Observation of Disorder-Induced Boundary Localization," *Proceedings of the National Academy of Sciences* 122, no. 19 (2025): e2422154122.

20. E. L. Weerda and M. Rizzi, "Fractional Quantum Hall States With Variational Projected Entangled-Pair States: A Study of the Bosonic Harper-Hofstadter Model," *Physical Review B* 109 (2024): L241117.

21. P. Mai, E. W. Huang, J. Yu, B. E. Feldman, and P. W. Phillips, "Interaction-Driven Spontaneous Ferromagnetic Insulating States With Odd Chern Numbers," *npj Quantum Materials* 7 (2022): 44.

22. M. Aidelsburger, M. Lohse, C. Schweizer, "Measuring the Chern Number of Hofstadter Bands With Ultracold Bosonic Atoms," *Nature Physics* 11 (2015): 162–166.

23. Y. Kuno, "Disorder-Induced Chern Insulator in the Harper-Hofstadter-Hatsugai Model," *Physical Review B* 100, no. 5 (2019): 054108.

24. Y.-F. Zhang, Y. Yang, Y. Ju, D. N. Sheng, and D.-Y. Xing, "Coupling-Matrix Approach to the Chern Number Calculation in Disordered Systems," *Physical Review B* 87, no. 20 (2013): 205136.

25. H.-C. Hsu, P.-M. Chiu, and P.-Y. Chang, "Disorder-Induced Topology in Quench Dynamics," *Physical Review B* 104, no. 5 (2021): 054201.

26. Y. Yang, Z. Zhang, and S.-Q. Shen, "Quantum Phase Transitions and Phase Diagram of the Topological Anderson Insulator," *Physical Review Letters* 107 (2011): 066602.

27. L. Ulčakar, J. Mravlje, and T. c. v. Rejec, "Kibble-Zurek Behavior in Disordered Chern Insulators," *Physical Review Letters* 125 (Nov 2020): 216601.

28. B. Andrews, T. Neupert, and G. Möller, "Stability, Phase Transitions, and Numerical Breakdown of Fractional Chern Insulators in Higher Chern Bands of the Hofstadter Model," *Physical Review B: Condensed Matter* 104 (Sep 2021): 125107.

29. T. Peng, Y.-C. Xiong, C.-B. Hua, et al., "Structural Disorder-induced Topological Phase Transitions in Quasicrystals," *Physical Review B: Condensed Matter* 109 (May 2024): 195301.

30. T. Tan and T. Devakul, "Parent Berry Curvature and the Ideal Anomalous Hall Crystal," *Physical Review X* 14, no. 4 (2024): 041040.

31. I. Bloch, J. Dalibard, and W. Zwerger, "Many-Body Physics With Ultracold Gases," *Reviews of Modern Physics* 80 (2008): 885–964.

32. S. Trotzky, P. Cheinet, S. Fölling, et al., "Time-Resolved Observation and Control of Superexchange Interactions With Ultracold Atoms in Optical Lattices," *Science* 319 (2008): 295–299.

33. M. Aidelsburger, M. Atala, M. Lohse, J. T. Barreiro, B. Paredes, and I. Bloch, "Realization of the hofstadter hamiltonian with ultracold atoms in optical lattices," *Physical Review Letters* 111 (2013): 185301.

34. M. Aidelsburger, M. Lohse, C. Schweizer, et al., "Measuring the Chern Number of Hofstadter Bands With Ultracold Bosonic Atoms," *Nature Physics* 11 (2015): 162–166.

35. M. Tarnowski, F. N. Ünal, N. Fläschner, B. S. Rem, A. Eckardt, K. Sengstock, and C. Weitenberg, "Measuring Topology From Dynamics by Obtaining the Chern Number From A Linking Number," *Nature Communication* 10 (2019): 1728.

36. Y. Cao, V. Fatemi, A. Demir, et al., "Correlated Insulator Behaviour at Half-Filling in Magic-Angle Graphene Superlattices," *Nature* 556, no. 7699 (Apr 2018): 80–84.

37. Y. Xie, B. Lian, B. Jäck, et al., "Spectroscopic Signatures of Many-body Correlations in Magic-Angle Twisted Bilayer Graphene," *Nature* 572, no. 7767 (Aug 2019): 101–105.

38. R. Bistritzer and A. H. MacDonald, "Moiré Bands in Twisted Double-Layer Graphene," *Proceedings National Academy of Science USA* 108 (2011): 12 233–12 237.

39. T. Ozawa, H. M. Price, A. Amo, et al., "Topological Photonics," *Reviews of Modern Physics* 91 (2019): 015006.

40. D. J. Thouless, M. Kohmoto, M. P. Nightingale, and M. den Nijs, "Quantized Hall Conductance in a Two-Dimensional Periodic Potential," *Physical Review Letters* 49 (1982): 405–408.

41. D. N. Sheng, Z. Y. Weng, L. Sheng, and F. D. M. Haldane, "Quantum Spin-Hall Effect and Topologically Invariant Chern Numbers," *Physical Review B: Condensed Matter* 80 (2009): 165316.

42. E. L. Weerda and M. Rizzi, "Fractional Quantum Hall States With Variational Projected Entangled-Pair States: A Study of the Bosonic Harper-Hofstadter Model," *Physical Review B: Condensed Matter* 109 (2024): 094202.